Luminescence and Photoconductivity studies on amorphous and nanocrystalline ZnO thin films obtained by sol-gel

J. A. García-Macedo [1*], G. Valverde-Aguilar[1], J. L. Manríquez-Zepeda[1]

1. Departamento de Estado Sólido. Instituto de Física, Universidad Nacional Autónoma de México. México D.F. C.P. 04510

*** Contact author:**
Dr. Jorge Garcia Macedo
Instituto de Física, UNAM
Circuito de la Inv. Científica s/n
C. P. 04510. Del. Coyoacán
México, D.F.
México.
Tel. (5255) 5622−51−03
Fax (5255) 5616−15−35
E−mail: gamaj@fisica.unam.mx

ABSTRACT

Amorphous and nanocrystalline ZnO thin films were synthesized by the sol–gel process at room temperature. The films were spin-coated on glass and silicon wafers and gelled in humid air. The ZnO films were synthesized by using zinc acetate dihydrate as the inorganic precursor. The samples were annealed at at 450°C for 15 minutes to produce a polycrystalline ZnO thin films. The films were characterized using X-ray diffraction, Fourier transform infrared spectroscopy, scanning electron microscopy and transmission electronic microscopy and UV-Vis absorption spectroscopy. The experimental absorption spectrum of the crystalline ZnO film exhibits an absorption band located at 359 nm. Emission and excitation studies of the ZnO nanocrystallites were made in both kinds of materials to determine its luminescence response. Photoconductivity studies were performed on amorphous and crystalline (wurtzite phase) films. The experimental data were fitted with straight lines at darkness and under illumination at 355 nm and 633 nm. This indicates an ohmic behavior. Transport parameters were calculated. Results are discussed.

KEYWORDS: Zinc oxide, semiconductor, sol-gel, thin film, wurtzite

1. INTRODUCTION

Zinc oxide (ZnO) has a wide and direct band gap of 3.36 eV at room temperature and a higher exciton binding energy (60 meV), which assures more efficient exciton emission at higher temperatures, compared with other wide band gap materials, such as GaN (28 meV) and ZnSe (19 meV) [1–3]. In addition, ZnO can be deposited at lower temperature than GaN. Owing to these properties, ZnO has received much attention as a candidate material for opto-electronic devices such as UV laser diodes and UV-blue light-emitting diodes.

ZnO has been studied in different growth forms such as nanoneedles, nanowires, nanorods, flowers, tetrapods, etc [4–8] for its luminescence properties. In particular, ZnO powders and thin films are very important materials in ceramic technology and thin films technology due to numerous properties [9]. ZnO powder with

Nanophotonic Materials VI, edited by Stefano Cabrini, Taleb Mokari, Proc. of SPIE Vol. 7393, 73930Q · © 2009 SPIE · CCC code: 0277-786X/09/$18 · doi: 10.1117/12.826720

suitable dopants is used as a photoconductor in electrophotography, a varistor in ceramic technology, a sensor element in sensing combustible gases and additive in various ferrites. As a thin film exhibits piezoelectric properties which are used in various pressure transducers and acousto-optic devices, surface and bulk acoustic wave devices, solar cells, piezoelectric transducers [10]. ZnO is a direct band gap semiconductor [11-13].

In the present work, we described the synthesis and characterization of amorphous and nanocrystalline ZnO thin films. The films were produced by the sol–gel process at room temperature by using the spin-coating method and deposited on glass substrates. The samples were sintered at 520°C for 1 hour. The obtained films were characterized by X-ray diffraction (XRD), optical absorption (OA), infrared spectroscopy (FTIR) and transmission electronic microscopy (TEM) studies. Photoconductivity studies were performed on amorphous and nanocrystalline (wurtzite phase) films. Transport parameters were calculated. The emission properties of amorphous and nanocrystalline ZnO samples were studied by luminescence studies.

2. EXPERIMENTAL

Silicon and glass substrates were cleaned in boiling acidic solution of sulphuric acid-H_2O_2 (4:1) under vigorous stirring for 30 minutes. They were then placed in deionized water and boiled for 30 minutes, rinsed three times with deionized water and stored in deionized water at room temperature.

All reagents were Aldrich grade. The sol was prepared using zinc acetate dihydrate ($Zn\text{-}(OOC\text{-}CH_3)_2{\cdot}2H_2O$), ethyleneglycol ($C_2H_60_2$), ethanol ($CH_3CH_2OH$), and glycerol ($C_3H_8O_3$). 2.5 ml of ethylene glycol was added to 10 g of zinc acetate dihydrate in a round bottomed flask fitted with a condenser and kept at 150 °C for 15 min over a hot plate to obtain a uniform transparent solution. On cooling to room temperature the content of the flask solidified to a transparent brittle solid which was dissolved in 20 ml ethanol, 0.5 ml of glycerol and 6.35 ml of triethylamine. The precursor solution was placed on the glass or silicon substrates (2.5 x 2.5 cm^2) using a dropper and spun at a rate of 3000 rpm for 20 s (Figure 1).

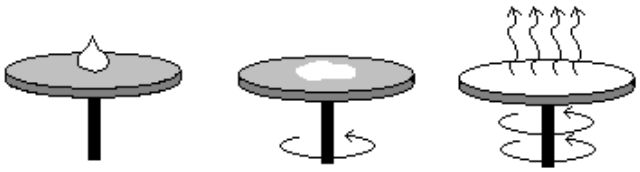

Figura 1. Spin-coating technique.

After coating, the precursor films were kept in humid air (RH 40%) for 10 min to facilitate hydrolysis. The films were dried at 450 °C for 15 min in a muffle oven in order to make them crystalline.

UV-vis absorption spectra were obtained on a Thermo Spectronic Genesys 2 spectrophotometer with an accuracy of ±1 nm over the wavelength range of 300-900 nm. The structure of the final films was characterized by X-ray diffraction (XRD) patterns. These patterns were recorded on a Bruker AXS D8 Advance diffractometer using Ni-filtered CuKα radiation. A step-scanning mode with a step of 0.02° in the range from 1.5 to 60° in 2θ and an integration time of 2 s was used. FTIR studies were done using a Bruker Tensor 27 FT-IR spectrometer.

Another characterization of the morphology and microstructure was achieved from conventional transmission electron microscopy (TEM) by means of a JEOL FEG 2010 FasTem electron microscope with 1.9 Å resolution (point to point). For TEM studies, the sample was suspended in ethanol in order to disperse the powders and a drop of the sample was deposited on a lacey carbon copper grid as a TEM support. From the TEM micrographs, mean particle size and particle size distribution were calculated, too. The thickness of the films was measured using a SEM microscopy Model STEREOSCAN at 20 kV.

For photoconductivity studies[9] silver electrodes were painted on the sample. It was maintained in a 10^{-5} Torr vacuum cryostat at room temperature in order to avoid humidity. For photocurrent measurements, the films were illuminated with light from an Oriel Xe lamp passed through a 0.25m Spex monochromator. Currents were measured with a 642 Keithley electrometer connected in series with the voltage power supply. The applied electrostatic field E was parallel to the film. Light intensity was measured at the sample position with a Spectra Physics 404 power meter (Figure 2).

Emission and excitation optical spectra were collected at room temperature with a SPEX FLUOROLOG FL111 spectrofluorimeter equipped with a 450Wxenon lamp. Excitation and emission wavelengths were selected

by two monochromators (SPEX spectrometer 0.34m), and the detection was done with a HAMAMATSU R928 photomultiplier tube.

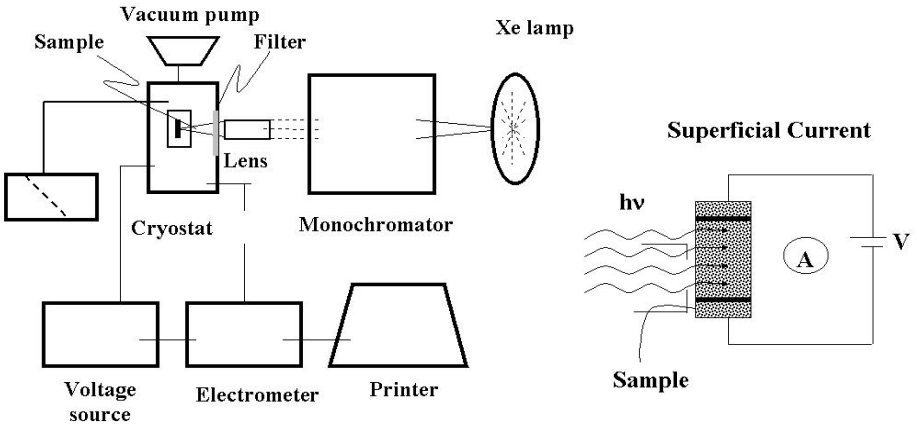

Figure 2. Schematic diagram of the photoconductivity technique. Superficial current was produced on the thin film when an electric field was applied to it.

3. RESULTS AND DISCUSSION

3.1 Optical absorption. Figure 3 shows the optical absorption spectra of the amorphous and crystalline ZnO thin films taken at room temperature in the range of 300-900 nm. The absorption spectrum of the amorphous film does not exhibit any band (grey line). The spectrum of the film calcined at 450 °C for 15 min (black line) shows an absorption band A located at 359 nm. This spectrum corresponds to the wurtzite phase.

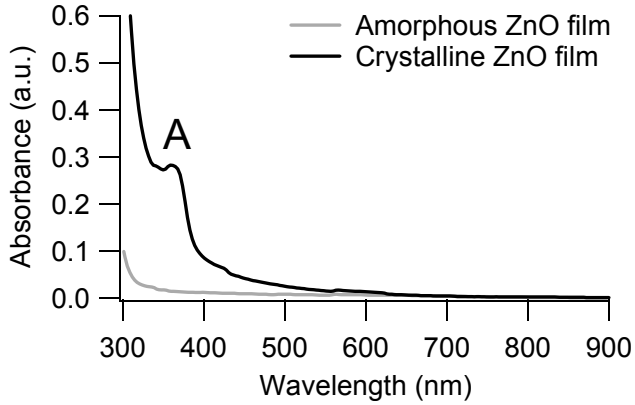

Figure 3. Absorption spectra of the ZnO/TiO_2 thin films. The spectrum for amorphous film corresponds to the gray line, and the nanocrystalline film sintered at 520 °C for 1 h corresponds to the black line.

The optical band-gap, Eg, was determined from the absorption spectrum (nanocrystalline film, Figure 3) using equation [14, 15]:

$$(\alpha h\nu)^2 = C(h\nu - E_g) \qquad (1)$$

where α is the absorption coefficient, $h\nu$ is the photon energy, E_g is the band gap energy and C depends on the electron-hole mobility.

The $(\alpha h\nu)^2$ vs. $h\nu$ plot is displayed in Figure 4. The value of E_g was determined plotting a tangent line (black solid line) to the curve. The obtained value of 3.18 eV (it is marked with a cross) is similar to the optical band-gap reported for similar monocrystalline ZnO films [16].

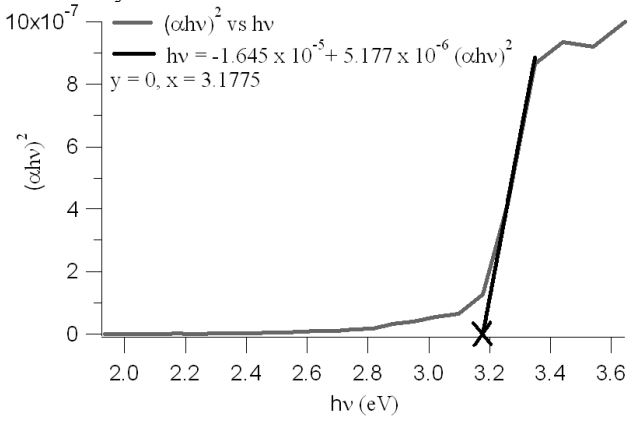

Figure 4. Evolution of the $(\alpha h\nu)^2$ vs. $h\nu$ curve of nanocrystalline ZnO film (grey solid line). The E_g value of 3.18 eV is marked with a cross.

3.2 Emission and Excitation Spectra. Room temperature luminescence emission spectra of ZnO nanocrystallites are shown in Figure 5. Their luminescent response is compared to those from amorphous films and the silicon wafer. The ZnO was excited at 359 nm, which corresponds to the maximum absorption value (Fig. 3). The samples show luminescence behaviour with a small violet emission A band located at 409 nm (3.03 eV) and narrow blue emission B and C bands located at 455-476 nm (2.72-2.60 eV). The D band located at 561 nm corresponds to the silicon wafer. The luminescence emission characteristics of ZnO films are strongly dependent on both the crystal quality of the film and the film stiochiometry [17]. The bands from crystalline film are stronger than those from amorphous one. The visible emission of the ZnO films is related to different intrinsic defects, such as oxygen vacancies, zinc vacancies, zinc interstitials, oxygen interstitials, and anti-site defect O_{Zn} [17].

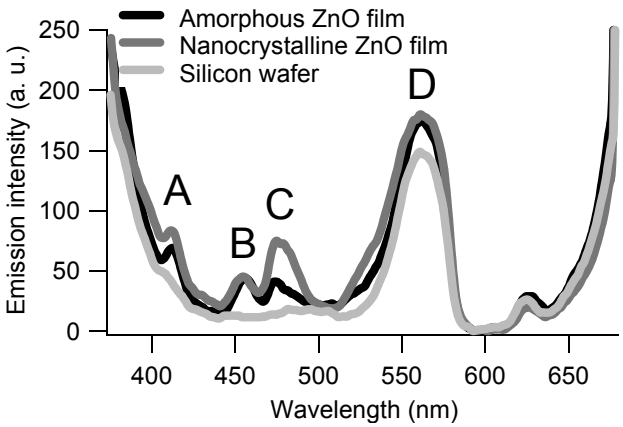

Figure 5. Emission spectra of nanocrystalline ZnO film (intense grey solid line) annealed at 450º C for 15 minutes, amorphous ZnO film (black dotted line) and silicon wafer (grey solid line). The spectra was obtained by using λ_{exc} = 359 nm.

Sun [18] calculated the energy levels of the intrinsic defects in ZnO applying full-potential linear muffin-tin orbital method and the results are depicted in Figure 6. From this figure, the energy of the transition from conduction band to the Zn vacancies (V_{Zn}) corresponds to the energy of 3.03 eV from the violet emission centered at 409 nm [19]. These vacancies are probably located at the grain boundaries. Blue band emission located at 476 nm (2.60 eV) from ZnO has been reported, but unfortunately the exact origins are not clear yet. The blue emission band of 455 nm (2.72 eV) can be originated from the electron transition from the shallow donor level of oxygen vacancies to the valence band [20]. Oxygen vacancies can produce two defect donor levels: one is the deep donor level located at 1.3–1.6 eV below the conductor band [21, 22], and the other is the shallow donor level below the conductor band at about 0.3–0.5 eV [23]. The energy interval from the shallow donor level to the top of the valence band is about 2.8 eV, which is consistent with the photon energy of the 2.72 eV blue emission observed in our study. Then, the 2.72 eV blue emission originated from the electron transition from the shallow donor level of oxygen vacancies to the valence band.

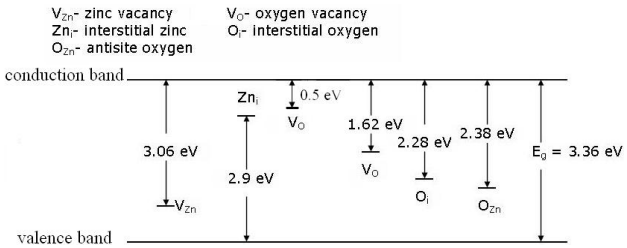

Figura 6. Schematic representation of calculated defect level in ZnO nanostructures.

Zinc interstitials also can be produced in zinc-rich samples, which are expected to act as donor centres. Calculations indicated that both oxygen vacancies and zinc interstitials had low formation energies [24, 25]. The energy level of zinc interstitials is located at 2.9 eV above the valence band for the samples with an energy gap of 3.36 eV [21]. For our sample, the energy gap is 3.18 eV, the energy level of zinc interstitials should be around 2.74 eV above the valence band, which is very close to the photon energy of the 2.72 eV blue emission observed in our study (Fig. 5). Therefore, the other origin of the blue emission can be the electron transition from the shallow donor level of zinc interstitials to the valence band.

Room temperature luminescence excitation spectra of ZnO nanocrystallites are shown in Figure 7. Their luminescent response is compared to those from amorphous film and the silicon wafer. The detection wavelengths λo were 410 nm, 455 nm and 475 nm. A broad band located around 350 nm is very close to the maximum absorption peak (359 nm).

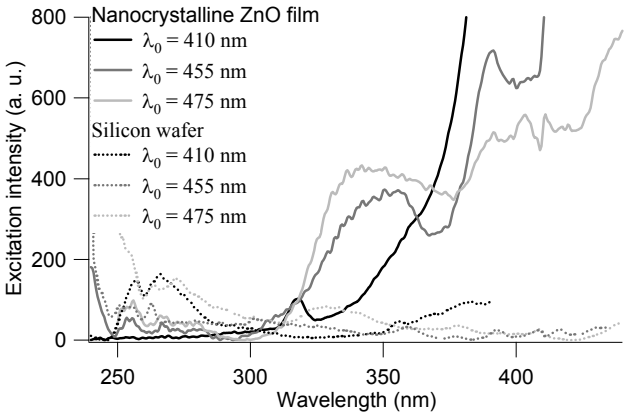

Figure 7. Excitation spectra of nanocrystalline ZnO film annealed at 450º C for 15 minutes, and silicon wafer. The spectra was obtained by using λ_0 = 410 nm, 455 nm and 475 nm.

3.3 X-ray diffraction. The X-ray diffraction patterns of the amorphous and nanocrystalline ZnO films are presented in Figure 8. The spectrum of amorphous film did not show any band. The films calcined at 450 °C for 15 minutes exhibit very good crystallization that corresponds to wurtzite form of ZnO formed by employing the sol-gel procedure. The diffraction peaks located at 2θ= 31.95, 34.60, 36.45, 47.65, 56.80, 62.95 and 68.00 can be indexed as (100), (002), (101), (102), (110), (103), (112) respectively. The position of the diffraction peaks in the film is in good agreement with those given in ASTM data card (#05-0664) for wurtzite form. The broad band located between 2θ = 20-40° corresponds to the glass substrate.

The average nanocrystalline size calculated using the diffraction peak [100] from Scherrer´s formula [26] was of 23 nm.

$$d = \frac{0.9\lambda}{B\cos\theta}$$

with λ=1.54056x10^{-10} m and B=0.4°=0.00628 rad.

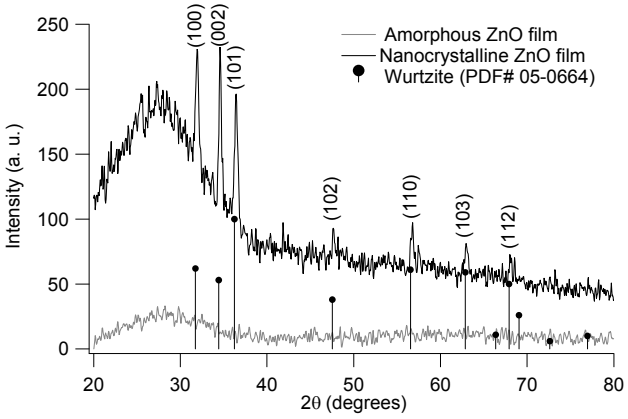

Figure 8. X-ray diffraction pattern at high angle of the nanocrystalline ZnO film sintered at 450 °C for 15 minutes.

3.4 HRTEM measurements. Figure 9 shows the HRTEM image of nanocrystalline ZnO film. It exhibits a population of small ZnO nanocrystallites. From HRTEM studies, the corresponding size-distribution histograms were obtained (Fig. 10). The distributions of the minor axis B and major axis A of the ZnO nanocrystallites are

very broad. The diameter values and standard deviations are A = 38.45 ± 15 nm (Fig. 10 a), B = 26.53 ± 9.54 nm (Fig. 10 b).

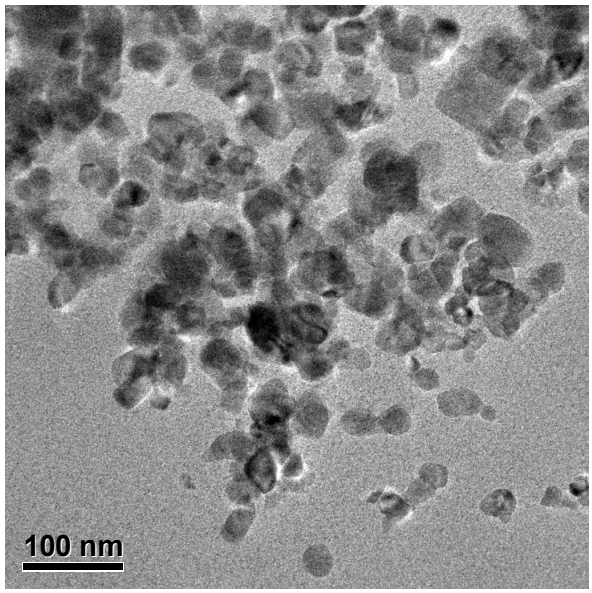

Figure 9. TEM image of nanocrystalline ZnO film.

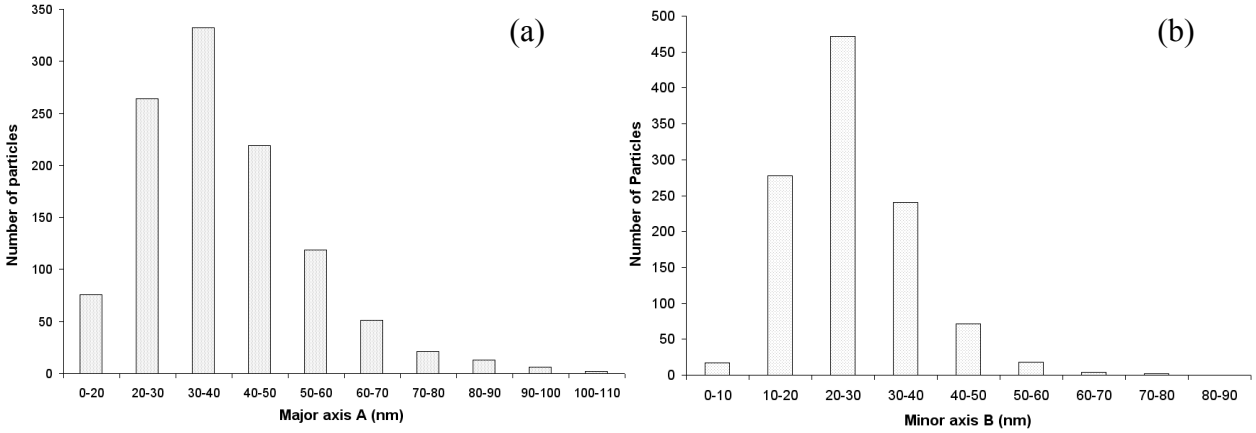

Figure 10. Size-distribution histograms obtained from HRTEM analysis of ZnO nanocrystallites.

The average diameter obtained by HRTEM is consistent with the value obtained by Scherrer´s formula.

The maximum absorption peak located at 359 nm can be due to an exitonic peak which is related to the quantum confinement effect due to nanoscopic size of the crystallites. The position of this peak depends on the grain size by the relation [15, 27]:

$$\frac{1240}{\lambda_{1/2}} = a + \frac{b}{D^2} - \frac{c}{D} \qquad (2)$$

where $\lambda_{1/2}$ corresponds to the wavelength at 50% of the peak intensity and the constants a = 3.301, b = 294, c = -1.09. These empiric values allow for a adequate description of the relation between $\lambda_{1/2}$ and crystallite size, D. The average value of D = 38.45 nm calculated by HRTEM measurements is substituted in the eq. 2 to obtain a value of $\lambda_{1/2}$ = 351.4 nm, which coincides with the maximum absorption peak. Therefore, not only a band gap is possible related with this absorption, but an exitonic transition.

.

3.5 FTIR spectra. Figure 11 shows FTIR spectra of amorphous and nanocrystalline ZnO samples prepared as KBr pellets. For both samples, the modes observed at 471 cm^{-1} (amorphous), 465 cm^{-1} (nanocrystalline) agree well with the the ZnO stretching mode [28]. For amorphous sample, the peaks at 854 and 1042 cm^{-1}, and for crystalline sample the peaks located at 865 and 1038 cm^{-1}; are attributed to symmetric and asymmetric bending and stretching modes of $ZnO \cdot H_2O$, respectively [28].

Acetate complexing ligand can form unidentate, bidentate (chelating) and bridging bonding structure with zinc ions [29], resulting in different stretching frequencies for the C=O (1557-1599 cm^{-1}) and C-O (1410 cm^{-1}) vibrations. Specifically, the band seen at 1557 cm^{-1} arises due to the bridging type metal-acetate bonding (M--OCOO-M). The band at 1342 crn^{-1} is due to weakly bound acetic acid molecule (HOOC-R).

In addition to the ethyl groups, isopropyl groups, the bands located at 2900-2945 cm^{-1} are C-H stretching. Table 1 contains the bands of amorphous and nanocrystalline ZnO samples and their description.

The band located at 1068 cm^{-1} corresponds to the solvent, ethanol. After the annealing treatment this band disappeared in the spectrum for nanocrystalline sample.

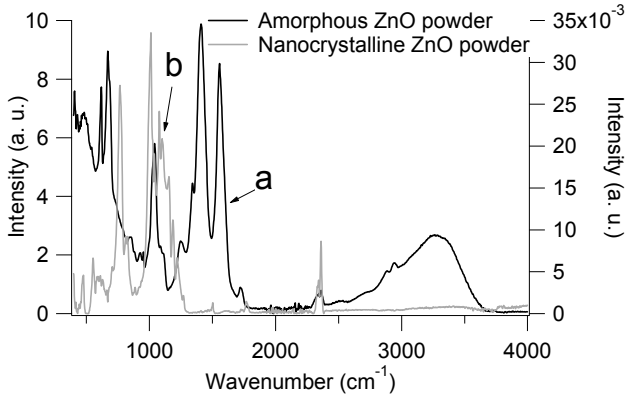

Figure 11. FTIR spectra of (a) amorphous ZnO sample, and (b) nanocrystalline ZnO sample annealed at 450 °C for 15 min. Both samples were prepared as KBr pellets.

Table 1. IR frequencies [in cm^{-1}], of the amorphous and nanocrystalline ZnO films.

Amorphous	Nanocrystalline	
$\bar{\nu}_{exp}$ (cm^{-1})	$\bar{\nu}_{exp}$ (cm^{-1})	description
471	465	ZnO stretching
854	865	symm. bending ZnO
1068	-	Ethanol
1042	1038	asymm. stretching ZnO
-	1121	-
1248	-	-
1342	-	HOOC-R
1410	-	C-O
1557	1599	C=O
2900	-	C-H stretching
2945	-	C-H stretching
3263	3414	H-O especies

3.6 Photoconductivity studies. Usually [30] Ohm's law under light illumination is given by

$$\vec{J} = \vec{J}_{ph} + (\sigma_d + \sigma_{ph})\vec{E}, \quad (3)$$

where $\vec{J}_{ph}$ is the photovoltaic current density, and σ_{ph} is the photoconductivity. When the current densities are assumed to be parallel to the electric field $\vec{E}$ Eq. (3) becomes into the next one:

$$J = \frac{q\phi l_0 \alpha I}{h\nu} + \left(\sigma_d + \frac{q\phi\mu\tau\alpha I}{h\nu}\right)E\,, \tag{4}$$

with ϕ as the quantum yield of charge carrier photogeneration, l_0 as the charge carrier mean free path, α as the sample absorption coefficient, I as the light intensity at the frequency ν of illumination, h as the Planck´s constant, and τ as the charge carriers mean lifetime. The first term is the photovoltaic transport effect, the second one is the dark conductivity $\sigma_d = en_0\mu$, and the third one is the photoconductivity itself.

Eq (4) can be written as:

$$J = A_1 E + J_0 \tag{5}$$

From the absorption spectrum of nanocrystalline film (Fig. 3), the illumination wavelength for photoconductivity studies were chosen: 355 nm that corresponds to the maximum absorption band and 633 nm were there is no absorption. Photoconductivity results of amorphous and nanocrystalline ZnO films are shown in Figure 12. Current density as function of electric applied field on the film was plotted. The experimental data were fitted by least-squares with straight lines at darkness and under illumination (355 nm, 633 nm). This indicates an ohmic behaviour. The linear fit for all samples are shown in Table 2.

In general, the slope A_1 from crystalline films is bigger than that from amorphous films. It indicates that the crystallization of the films improves their photovoltaic and photoconductive properties. The fits are included in the Table 2. For crystalline samples, when the illumination wavelength decreases the slope decreases. On the other hand, for amorphous films this effect is opposite.

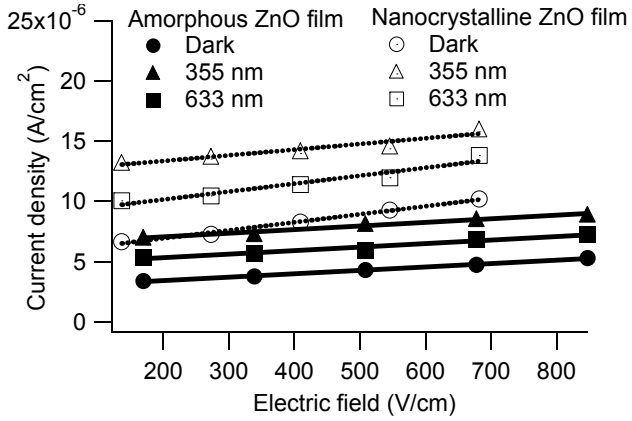

Figure 12. Current density vs. electric field spectra from amorphous ZnO film (solid lines), and nanocrystalline ZnO film (dotted lines).

Table 2. Linear fittings of amorphous and nanocrystalline ZnO films.

λ (nm)	Film	A_1	J_0
633	Amorphous	2.93×10^{-9}	4.73×10^{-6}
	Nanocrystalline	6.62×10^{-9}	8.84×10^{-6}
355	Amorphous	2.99×10^{-9}	6.46×10^{-6}
	Nanocrystalline	4.71×10^{-9}	1.24×10^{-5}
Darkness	Amorphous	2.82×10^{-9}	2.86×10^{-6}
	Nanocrystalline	6.69×10^{-9}	5.59×10^{-6}

With the equation (4), by measuring I, the dark conductivity and the conductivity under illumination at 633 and 355 nm, and fitting the experimental data by the least squares method, as it is shown in Fig. 12, the photoconductive ($\phi\mu\tau$) and photovoltaic (ϕl_0) parameters were obtained (Table 3).

Table 3. Photovoltaic and photoconductive parameters of amorphous and nanocrystalline ZnO films.

Sample	Parameter	633 nm	355 nm
Amorphous	ϕl_0 (cm)	2.5×10^{-6}	2.2×10^{-6}
	$\phi\mu\tau$ (cm^2/V)	1.5×10^{-10}	1.0×10^{-10}
Nanocrystalline	ϕl_0 (cm)	8.8×10^{-6}	0.2×10^{-6}
	$\phi\mu\tau$ (cm^2/V)	0.0046×10^{-10}	0.6×10^{-10}

The photovoltaic parameter (ϕl_0) decrease when the wavelength diminishes. This also happens with the photoconductive parameter ($\phi\mu\tau$) in the amorphous films, but it increases in the crystalline films indicating an efficient photoconductive behaviour. For amorphous films, $\phi\mu\tau$ parameter is bigger than that for crystalline one. This is probably due to the high content of solvents in the amorphous films, which increases their conductivity.

4. CONCLUSIONS

High optical quality amorphous and nanocrystalline ZnO films were obtained by sol-gel process. An energy band gap of 3.18 eV was obtained. FTIR studies indicate that the bands 1068, 1335, 1582 and 2851 cm^{-1} disappeared after the annealing treatment. HRTEM measurements determined that the dominant specie of ZnO nanocrystals has diameters between 30- 40 nm. The nanoscopic size of the crystallites (D = 38.45 nm) determined the position of the exitonic peak 359 nm which is related to the quantum confinement effect.

The intensity of the luminescent emission depends of the film crystallization. This is more intense in the nanocrystalline films than the amorphous ones. The strongest transitions are located at 409 nm, 455 nm and 475 nm corresponding to the zinc vacancies (V_{Zn}), to electronic transitions of the oxygen vacancies and zinc interstitials, and unknown origin, respectively.

Photoconductivity studies on these films were done. The wurtzite phase obtained in the ZnO matrix provides more stability that improves the photoconductivity. In the nanocrystalline films when the illumination wavelength decreases the photoconductive parameter increases. This effect indicates a strong photoconductive behaviour. For amorphous films, $\phi\mu\tau$ parameter is bigger than that for the crystalline ones. This is probably due to the high content of solvents in the amorphous films, which increases their conductivity.

ACKNOWLEDGMENTS

The authors acknowledge the financial supports of CONACYT 79781, CONACyT 89584, NSF-CONACYT, PUNTA, ICYTDF and PAPIIT 116506-3. GVA is grateful for ICyTDF postdoctoral fellowship. The authors are thankful to M. in Sci. Manuel Aguilar-Franco (XRD), Luis Rendón (HRTEM), Roberto Hernández- Reyes (SEM) and Diego Quiterio (preparation of the samples for SEM studies) for technical assistance.

REFERENCES

[1] Yoshino, K., Yoneta, M., Saito, H., Ohishi, M., Chan, L. H., Abe, T., Ando, K., Ikari, T., "Photoluminescence and photoacoustic spectra of N-doped ZnSe epitaxial layers grown by molecular beam epitaxy", J. Cryst. Growth 214–215, 572-575 (2000).

[2] Li, X., Shao, C., Qiu, S., Xiao, F. S., Zheng, W., Liu, Z., Terasaki, O., "Blue photoluminescence from SiC nanopartciles encapsulated in ZSM-5", Mater. Lett. 48(3-4), 242-246 (2001).

[3] Look, D. C., "Recent advances in ZnO materials and devices", Mater. Sci. Eng. B 80(1-3), 383-387 (2001).

[4] Murray, C. B., Norris, D. J., Bawendi, M. G., "Synthesis and characterization of nearly monodisperse CdE (E = sulfur, selenium, tellurium) semiconductor nanocrystallites", J. Am. Chem. Soc. 115(19), 8706-8715 (1993).

[5] Nirmal, N., Dabbousi, B. O., Bawendi, M. G., Macklin, J. I., Trautman, J. K., Harris, T. D., Brus L. E., "Fluorescence intermittency in single cadmium selenide nanocrystals", Nature 383, 802-804 (1996).

[6] Empedocles, S. A., Norris, D. J., Bawendi, M. G., "Photoluminescence spectroscopy of single CdSe nanocrystallite quantum dots", Phys. Rev. Lett. **77**(18), 3873-3876 (1996).
[7] Matsuura, D., Kanemitsu, Y., Kushida, T., White, C. W., Budai, J. D., Meldrum, A., "Optical characterization of CdS nanocrystals in Al2O3 matrices fabricated by ion-beam synthesis", Appl. Phys. Lett. **77**(15), 2289-2291 (2000).
[8] Efros, A. L., Rosen, M., "Random Telegraph Signal in the Photoluminescence Intensity of a Single Quantum Dot", Phys. Rev. Lett. 78(6), 1110-1113 (1997).
[9] Kamalasanan, M. N., Chandra, S., "Sol-gel síntesis of ZnO thin films", Thin Solid Films 288(1-2), 112-115 (1996).
[10] Tai, W.-P., Oh, J.-H., "Humidity sensing behaviors of nanocrystalline Al-doped ZnO thin films prepared by sol-gel process", Journal of Materials Science 13(7), 391-394 (2002).
[11] Marci, G., Augugliaro, V., Lopez-Munoz, M. J., Martin, C., Palmisano, L., Rives V., "Preparation, characterization and photocatalytic activity of Polycrystalline ZnO/TiO_2 systems. 2. Surface, bulk characterization, and 4-nitrophenol photodegradation in liquid–solid regime", J. Phys. Chem. B 105(5), 1033–1040 (2001).
[12] Hsu, C. C., Wu, N. L., "Synthesis and photocatalytic activity of ZnO/ZnO_2 composite", J. Photochem. Photobiol. A Chem 172(3), 269–274 (2005).
[13] Zhang, D. K., Liu, Y. C., Liu, Y. L., Yang, H., "The electrical properties and the interfaces of CuO/ZnO/ITO p–i–n heterojunction", Physica B 351(1-2), 178–183 (2004).
[14] Tauc, J., Grigorovichi, R., Vancu, A., "Optical properties and electronic structure of amorphous germanium", Phys. Status Solidi. 15, 627–633 (1966).
[15] Valle, G. G., Hammer, P., Pulcinelli, S. H., Santilli, C. V., "Transparent and conductive ZnO:Al thin films prepared by sol-gel dip-coating", Journal of the European Ceramic Society 24(6), 1009–1013 (2004).
[16] Bonamali, P., Maheshwar, S., "Enhanced photocatalytic activity of highly porous ZnO thin films prepared by sol–gel process", Mater. Chem. and Phys. 76(1), 82–87 (2002).
[17] Jeong, S.-H., Kim, B.-S., Lee, B.-T., "Photoluminescence dependence of ZnO films grown on Si (100) by radio-frequency magnetron sputtering on the growth ambient", Appl. Phys. Lett. 82(16), 2625-2627 (2003).
[18] Sun, Y. M., Ph. D. Thesis, University of Science and Technology of China, (2000).
[19] Kale, R. B., Hsu, Y.-J., Lin, Y.-F., Lu, S.-Y., "Synthesis of stoichiometric flowerlike ZnO nanorods with hundred per cent morphological yield", Solid State Commun. 142(5), 302–305 (2007).
[20] Zhang, D. H., Xue, Z. Y., Wang, Q. P., "The mechanisms of blue emission from ZnO films deposited on glass substrate by r.f. magnetron sputtering"; J. Phs. D: Appl. Phys. 35(21), 2837–2840 (2002).
[21] Lin, B. X., Fu, Z. X., Jia, Y. B., "Green luminescent center in undoped zinc oxide films deposited on silicon substrates", Appl. Phys. Lett. 79(7), 943-945 (2001).
[22] Xu, P. S., Sun, Y. M., Shi, C. S., Xu, F. Q., Pan, H. B., "Native Point Defect States in ZnO**",** Chin. Phys. Lett. 18(9), 1252-1253 (2001).
[23] Fu, Z. X., Guo, C. X., Lin, B. X., Liao, G. H., "Cathodoluminescence of ZnO Films", Chin. Phys. Lett. 15(6), 457-459 (1998).
[24] Zhang, S. B., Wei, S. H., Zunger, A., "Intrinsic n-type versus p-type doping asymmetry and the defect physics of ZnO", Phys. Rev. B 63(7), Art. 075205 (2001).
[25] Oba, F., Nishitani, S. R., Isotani, S., Adachi, H., Tanaka, I., "Energetics of native defects in ZnO", J. Appl. Phys. 90(2), 824-828 (2001).
[26] Wilson, G. J., Matijasevich, A. S., G. Mitchell, D. R., Schulz, J. C., Will, G. D., "Modification of TiO_2 for Enhanced Surface Properties: Finite Ostwald Ripening by a Microwave Hydrothermal Process", Langmuir 22(5), 2016-2027 (2006).
[27] Meulenkamp; E. A., "Síntesis and growth of ZnO nanoparticles"; J. Phys. Chem. B 102(29), 5566-5572 (1998).
[28] Wang, Z., Zhang, H., Wang, Z., Zhang, L., Yuan, J., "Structure and strong ultraviolet emission characteristics of amorphous ZnO films grown by electrophoretic deposition", J. Mater. Res. 18(1), 151-155 (2003).
[29] Tokumoto, M. S., Briois, V., Santilli, C. V., Pulcinelli, S. H., "Preparation of ZnO Nanoparticles: Structural Study of the Molecular Precursor", J. Sol-gel Sci. & Techn. 26, 547-551 (2003).
[30] García M., J., Mondragón, A., Hernández, J. M., Maldonado R., J. L., "Photocurrent determination of charge transport parameters in $KNbO_3:Fe^{3+}$", Opt. Mat. 3(1), 61-64 (1994).